JOURNAL OF Materials CHEMISTRY

Ferro-, ferri- and antiferro-electric behaviour in a bent-shaped mesogen

Avtar S. Matharu,*[a] Chrissie Grover,[a] Lachezar Komitov[b] and Gunnar Andersson[b]

[a]*Department of Chemistry and Physics, The Nottingham Trent University, Clifton Lane, Nottingham, UK NG11 8NS. E-mail: avtar.matharu@ntu.ac.uk*
[b]*Department of Microelectronics and Nanoscience, Chalmers Institute of Technology, S-412 96, Göteborg, Sweden*

Received 6th January 2000, Accepted 22nd March 2000
Published on the Web 4th May 2000

The synthesis of a novel bent-shaped, four-ring thiophene-based chiral liquid crystalline ester derived from 5-(4-*n*-decyloxyphenyl)thiophene-2-carboxylic acid and (*S*)-1-methylheptyl 4′-hydroxybiphenyl-4-carboxylate is reported, *i.e.*, (*S*)-4′-(1-methylheptyloxycarbonyl)biphenyl-4-yl 5-(4-*n*-decyloxyphenyl)thiophene-2-carboxylate. Optical microscopy, differential scanning calorimetry, miscibility study, and complementary electro-optical and current response studies reveal the existence of the SmA*, SmC*ferroelectric, SmC*ferrielectric, SmC*antiferroelectric and SmI*antiferroelectric phase types. Another mesophase type possibly exists below SmI*antiferroelectric which generates a rapid electro-optic response. Comparison with the analogous three-ring compound, *i.e.*, (*S*)-4-(1-methylheptyloxycarbonyl)phenyl 5-(4-*n*-decyloxyphenyl)thiophene-2-carboxylate increases the thermal stability by 95.8 °C and the SmI*antiferroelectric phase is observed in addition.

Introduction

Following the recent 17th International Liquid Crystal Conference, Strasbourg, France,[1] the area of design, synthesis and properties of ferri- and antiferro-electric liquid crystals attracted considerable attention. Compounds that exhibit these properties were first reported by Chandani *et al.*[2] in 1989. The antiferroelectric phase is particularly important because it participates in tristate switching *via* a very sharp electric field threshold.[3] In some instances, the electric field threshold may be absent or minimal in which case the switching process is said to be thresholdless.

The majority of compounds that exhibit the ferri- and antiferro-electric phase types are based on the conventional calamitic structural geometry, *i.e.*, linear and lath-like, and readily employ 1,4-disubstituted phenylene rings. However, there are relatively few examples reported in the literature based on either a bent or non-linear molecular architecture.[4]

Thiophene is a five-membered heterocycle containing sulfur which readily undergoes electrophilic aromatic substitution at either the α- or 2-, 5-positions (*ortho*- to the sulfur atom). Such a disposition of substituents generates an exocyclic bond angle of 148° which gives rise to a bend in the molecule. The central sulfur atom creates a strong transverse dipole moment, which may favour polar ordering. The exocyclic bond angle is intermediate between those for 1,4- (180°) and 1,3-phenylene (120°) and compounds comprising thiophene are expected to maintain mesomorphic properties. Hence, thiophene appears to be a natural choice for the study of bent-shaped molecules and is exemplified by Byron *et al.* in a recent publication.[5]

In this study, we aim to combine the attributes of shape geometry with chirality by investigating the occurrence of ferro-, ferri-, and antiferro-electricity in a four-ring thiophene-based chiral ester. To this effect, we now report the synthesis and characterisation (optical microscopy: glass slide and coverslip, and free standing films, miscibility study, differential scanning calorimetry, and complementary electro-optical and current response studies) of (*S*)-4′-(1-methylheptyloxycarbonyl)biphenyl-4-yl 5-(4-*n*-decyloxyphenyl)thiophene-2-carboxylate, **1**. The liquid crystalline properties will be compared with the analogous three-ring compound reported previously, *i.e.*, (*S*)-4-(1-methylheptyloxycarbonyl)phenyl 5-(4-*n*-decyloxyphenyl)thiophene-2-carboxylate.[5] The inclusion of an extra 1,4-disubstituted phenyl ring is expected to increase mesophase thermal stability either with retention, reduction or increase in the number of phase types. We envisage that the increase in thermal stability will induce the occurrence of phase types which appear below the SmC*antiferroelectric phase, *e.g.*, either SmI*antiferroelectric and/or high order crystal phases.

Results and discussion

Synthesis

The synthetic pathway for the preparation of compound **1** is summarised in Scheme 1. Chiral phenol, **6**, was prepared according to the method reported by Booth *et al.*[6]

4-*n*-Decyloxyphenylboronic acid, **3**, was prepared from its corresponding 4-*n*-decyloxy-1-bromobenzene, **2**, *via* low temperature lithiation (−78 °C) followed by trimethyl borate quench. Palladium-catalysed cross-coupling[7] of the boronic acid, **3**, with commercial 2-bromothiophene afforded the intermediate 2-(4-*n*-decyloxyphenyl)thiophene, **4**, which was then lithiated and treated with solid carbon dioxide to afford the desired carboxylic acid, **5**. Esterification[8] of compound **5**, in the presence of 1,3-dicyclohexylcarbodiimide (DCC) and 4-dimethylaminopyridine (DMAP) as catalyst, with (*S*)-1-methylheptyl 4′-hydroxybiphenyl-4-carboxylate, **6**, furnished the desired (*S*)-4′-(1-methylheptyloxycarbonyl)biphenyl-4-yl 5-(4-*n*-decyloxyphenyl)thiophene-2-carboxylate, **1**.

Optical microscopy, differential scanning calorimetry, miscibility study

Table 1 lists the mesomorphic transition temperatures and thermodynamic data for compound **1**. The optical studies were performed using a Nikon OPTIPHOT2-POL polarising microscope equipped with a Sony Hyper HAD SSC-DC38P digital video camera interfaced to a computer for direct image processing and storage, and a Mettler FP52 hot stage and FP5 control unit. Thermodynamic data were recorded using a Perkin-Elmer DSC7 differential scanning calorimeter. Textural

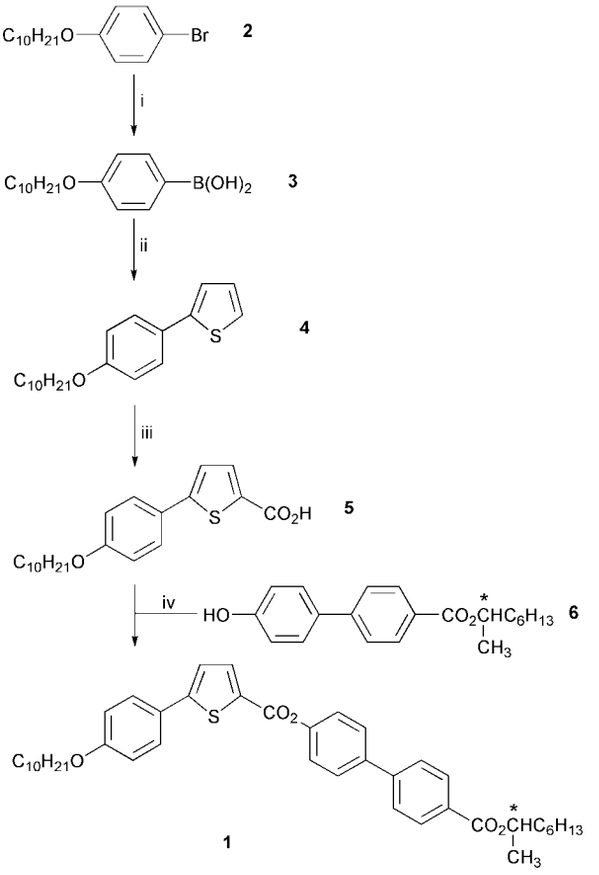

Scheme 1 Reagents and conditions: i, 1.6 M BuLi, then $B(OMe)_3$, −78 °C; ii, 2-bromothiophene, $Pd(PPh_3)_4$, 2 M Na_2CO_3, reflux; iii, 1.6 M BuLi, then CO_2, −78 °C to room temp.; iv, DCC, DMAP, CH_2Cl_2.

investigation of the phase types was undertaken both by viewing the sample confined between a glass slide and coverslip, and as a free-standing film.

In the case of the sample contained between a glass slide and a coverslip, on cooling from the isotropic liquid the SmA* phase was readily characterised by the appearance of focal-conic fans interspersed within a predominantly homeotropic texture (Fig. 1). The appearance of a vivid blue colouration (selective reflection) in the previously homeotropic regions coupled with formation of faint arcs across the focal-conic fans marked the onset of the SmC*ferroelectric phase (Fig. 2a). However, the real or true onset of the phase transition may have occurred earlier but could not be detected optically because it probably has a pitch that is shorter than the wavelength of visible light. The colour in the pseudohomeotropic region changes dramatically from an initial blue to green/red and then back to blue as the material is cooled. Such colour changes at a simplistic level show the temperature dependence of the pitch but interestingly also reveal that the material changes from short pitch (blue) to long pitch (red) and back to short pitch (blue). It must be stressed that the onset of the blue colouration on cooling may also be due to pre-

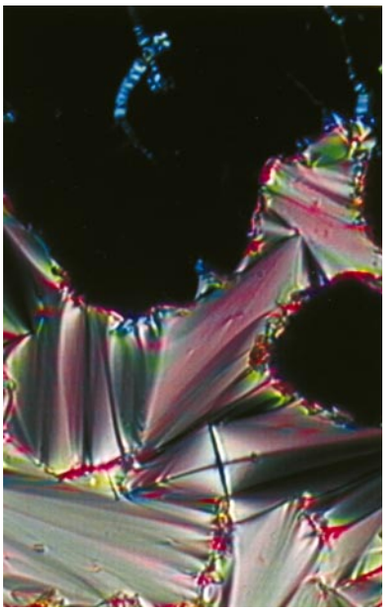

Fig. 1 Focal-conic fan and homeotropic texture (dark) of the SmA* phase.

transitional effects associated with the SmC*ferroelectric–SmC*ferrielectric transition. The SmC*ferrielectric phase was characterised by the appearance of a highly mobile, turbulent, milky-white texture in the pseudohomeotropic region together with disruption of the focal-conic fan texture (Fig. 3a). Shortly afterwards, the intense shimmering ceased to leave a 'homeotropic area' reminiscent of the SmA* phase but instead corresponds to the SmC*antiferroelectric phase (Fig. 4a). As the temperature is decreased, the arcs across the backs of the fans become more pronounced and the pseudohomeotropic region becomes mobile and exhibits a silver–grey luminescent texture. Prior to the onset of the next transition, a highly mobile, golden-yellow schlieren-mosaic-like texture develops which then clears to leave a very faint dull schlieren-mosaic-like texture with pronounced band/arc formation across the fans. At this stage, due its rather confusing texture, *i.e.*, similarities both of a smectic liquid crystal phase and a smectic crystal phase, the identity of this phase type could not be determined with any assurance. As reported later, a miscibility study using free-standing films was undertaken to ascertain the true identity of this phase type. The presence of a mosaic texture with strong grain boundaries in the free-standing film would be indicative of a high order smectic crystal phase. However at this stage this phase was tentatively assigned as SmI* due to the presence of a schlieren-mosaic-like texture which was difficult to bring in to optical focus (Fig. 5a). Thereafter, a granular texture began to form slowly across the fans suggesting either the onset of *crystallisation* evidenced by a large enthalphy of transition (15.2 kJ mol^{-1}) as detected by DSC or a high order smectic crystal phase (Fig. 6a). However, the latter seems more feasible as an electro-response is detected in this phase (see later).

Usually a textural study of this type is adequate for

Table 1 Liquid crystal transition temperatures (°C)[a] and enthalpy data (kJ mol^{-1})[a] for (*S*)-4′-(1-methylheptyloxycarbonyl)biphenyl-4-yl 5-(4-*n*-decyloxyphenyl)thiophene-2-carboxylate **1**

I–SmA*	SmA*–SmC*ferro	SmC*ferro–SmC*ferri	SmC*ferri–SmC*anti	S_C*anti–SmI*anti	SmI*anti–'SmX'
193.2	183.2[c]	159.6[c]	158.3[c]	106[c]	53.2[c]
[7.6]	[0.69]	[—][b]	[—][b]	[1.38]	[15.2]

[a]The first row gives transition temperatures and the second row [in square brackets] gives enthalpies of transition on cooling (DSC scan rate 10 °C min^{-1}). [b]The enthalpy of transition was too small to be evaluated. [c]Transition temperature determined from free standing film at a cooling rate of 1 °C min^{-1}.

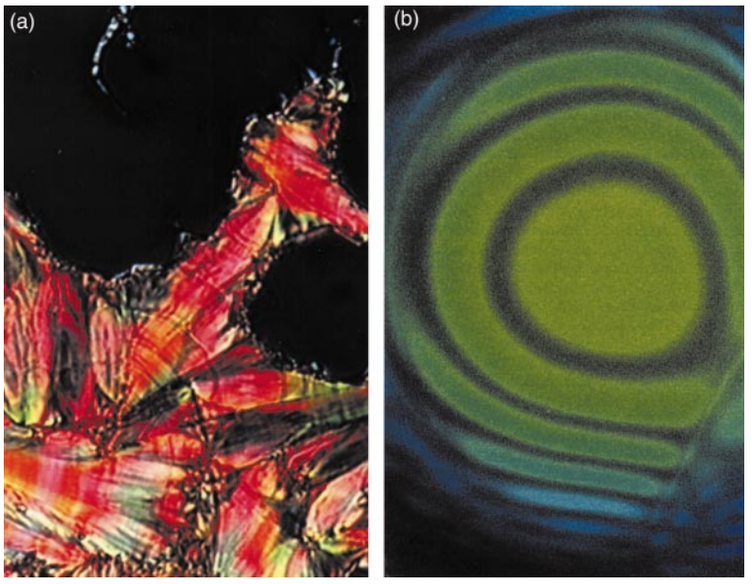

Fig. 2 Optical textures of the SmC*ferroelectric phase: (a) sandwich cell and (b) free-standing film.

mesophase identification and determination of transition temperatures. However determination of precise temperatures for the occurrence of the ferri- and antiferro-electric phase types is difficult because of strong and differing boundary conditions imposed by the glass substrates of the sandwich cell. Such forces can either induce or destroy the ferrielectric phase, and lead to problems of co-existence with either the ferroelectric and/or antiferroelectric phases. To minimise the influence of boundary conditions, optical textures and transition temperatures were further determined using the free-standing film technique.

The sample was heated to the SmA* phase and stretched across a 1 mm diameter hole, pre-drilled in a copper plate, using the edge of a coverslip. On cooling from the SmA* phase which obviously appears optically extinct between crossed polarisers, the SmC*ferroelectric phase appeared as a spectacular blue–green haze (Fig. 2b). Onset of continuous shimmering marked the transition to the SmC*ferrielectric phase (Fig. 3b). As the shimmering stopped, a clear film developed (pseudohomeotropic) characteristic of the SmC* antiferroelectric phase (Fig. 4b). Further cooling of the SmC* antiferroelectric phase produced a rather peculiar fingerprint texture which soon cleared to leave a schlieren-mosaic-like texture characteristic of the SmI*antiferroelectric (Fig. 5b) phase. The fingerprint texture may be due either to molecular re-ordering as a consequence of the transition or a possible helix inversion. This texture is quite different to transition bars or the inversion lines reported by Loubser *et al.*,[9] but similar to the textures reported by Gorecka *et al.*[10] We are currently undertaking elaborate pitch measurement studies to ascertain further the origin of this peculiar finger-print texture. Thereafter, a granular texture developed in the free-standing film (Fig. 6b) which may be onset of slow crystallisation or a high order smectic crystal phase.

Miscibility study, investigating the optical texture of each mixture as a free standing film, with (*S*)-1-methylheptyl 4-(4′-nonyloxybiphenyl-4-ylcarbonyloxy)benzoate, **7**, as the standard material[11] [transitions/°C: iso 142.2, SmA* 118.0,

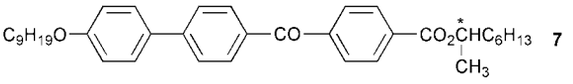

7

Fig. 3 Optical textures of the SmC*ferrielectric phase: (a) sandwich cell and (b) free-standing film.

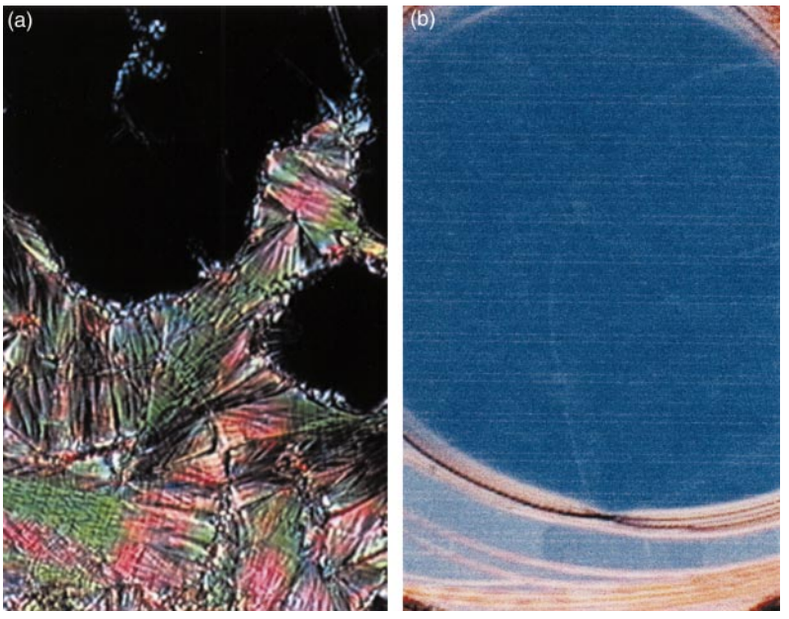

Fig. 4 Optical textures of the SmC*antiferroelectric phase: (a) sandwich cell and (b) free-standing film.

SmC*ferroelectric 112.0, SmC*ferrielectric 105.0, SmC*antiferroelectric 58.0, SmI*antiferroelectric] reveals continuous miscibility of the SmC*ferroelectric, SmC*ferrielectric, SmC*antiferroelectric and SmI*antiferroelectric phases across the entire composition range (Fig. 7).

Comparative study

Comparison of the thermal properties of compound **1** with the analogous three-ring compound reported previously, *i.e.*, (*S*)-4-(1-methylheptyloxycarbonyl)phenyl 5-(4-*n*-decyloxyphenyl)thiophene-2-carboxylate[5] [transitions/°C: iso 97.4, SmA* 92.2, SmC*ferroelectric 81.4, SmC*ferrielectric 78.8, SmC*antiferroelectric 48.6 cryst.] reveals that the inclusion of an extra 1,4-disubstituted phenyl ring increases mesophase thermal stability by 95.8 °C. In addition, an extra phase is observed, namely the SmI*antiferroelectric. However, it is unwise to make comparisons of the thermal properties of the SmC*ferri- and SmC*antiferro-electric phases because it is well known that both are affected by subtle changes in optical purity. Compound **1** and (*S*)-4-(1-methylheptyloxycarbonyl)phenyl 5-(4-*n*-decyloxyphenyl)thiophene-2-carboxylate were prepared using high purity (*R*)-octan-2-ol but from different batches. Hence we can not guarantee identical optical purity which invalidates the comparison of ferri- and antiferro-electric thermal stability.

Electro-optic and current response studies

The apparent tilt angle, spontaneous polarisation, electro-optic and current response were studied in glass cells consisting of two parallel glass plates with inner surfaces coated with a transparent conductive layer of indium tin oxide (ITO). The distance between the two plates was kept constant by spacers of 2 μm thickness. On the inner surface of the ITO layer, a polyimide alignment layer was deposited which was then rubbed unidirectionally in order to achieve the bookshelf geometry, *i.e.*, smectic layers perpendicular with respect to the glass substrates. The liquid crystal material was heated in to the isotropic liquid and allowed to enter the cell *via* capillary

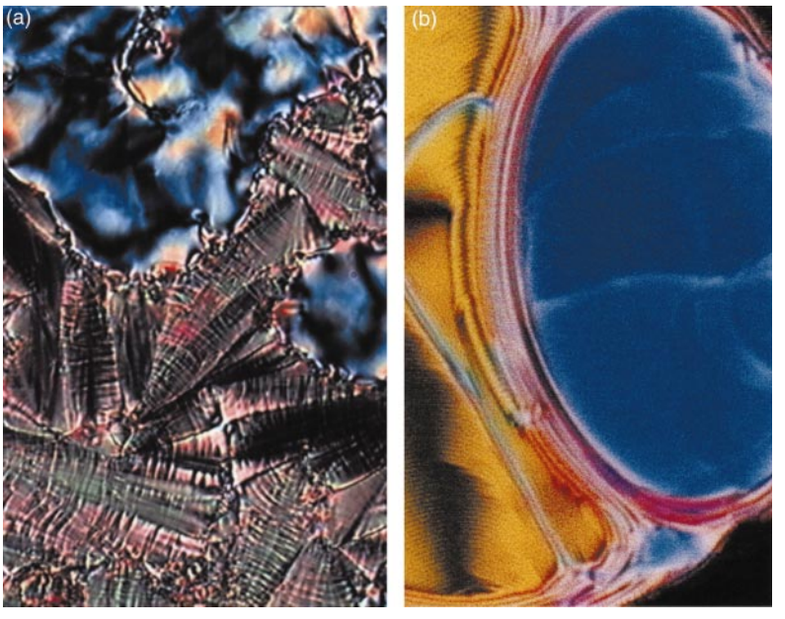

Fig. 5 Optical textures of the SmI*antiferroelectric phase: (a) sandwich cell and (b) free-standing film (emerging from RHS).

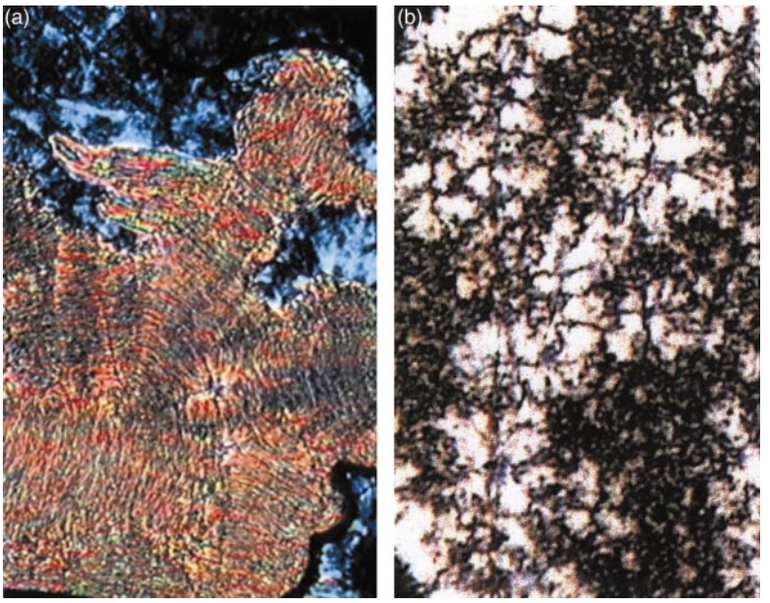

Fig. 6 Optical textures of the 'SmX' phase: (a) sandwich cell and (b) free-standing film.

action. The cell was inserted in a Mettler FP52 hot stage with temperature control within $\pm 0.1\,^{\circ}C$. The electro-optic responses of the samples were studied between cross-polarisers with sample optic axis oriented at 22.5° with respect to one of the polarizers.

The apparent tilt angle, θ_{app}, was measured as a half of the angle, α, between the positions of the sample optic axis corresponding to different field polarity. Angle α was found simply by rotating the sample between the cross polarisers and detecting the positions of two consecutive minima in the intensity of the light transmitted through the sample. The spontaneous polarisation, P_S, was measured according to the capacitance bridge method.[12] The applied voltage was kept high enough to ensure complete saturation of the ferroelectric switching.

The temperature dependence of the apparent tilt angle, θ_{app}, is shown in Fig. 8, and reveals a rather large maximum apparent tilt angle of approximately 37°. On cooling, θ_{app} increases continuously in the SmC* phase region whereas, in the SmC* ferri- and antiferro-electric phases, saturation at different levels is observed.

As shown in Fig. 9, the temperature dependence of the P_S at 100 °C reveals a maximum value of approximately 160 nC cm^{-2}. Fig. 10 shows the voltage dependence of the P_S at 158.5 °C and reveals the presence of the ferrielectric phase. Initially at low voltages, the P_S rises sharply (helix unwinding) and then reaches a short-lived plateau ($P_S = 70$ nC cm^{-2}; threshold voltage, $V_C = 8$ V) indicative of the ferrielectric state. Thereafter, the P_S continues to increase (field-induced transition of the ferri- to the ferro-electric state) before reaching a second stable saturation point (field-induced ferroelectric state) with P_S approximately 120 nC cm^{-2}.

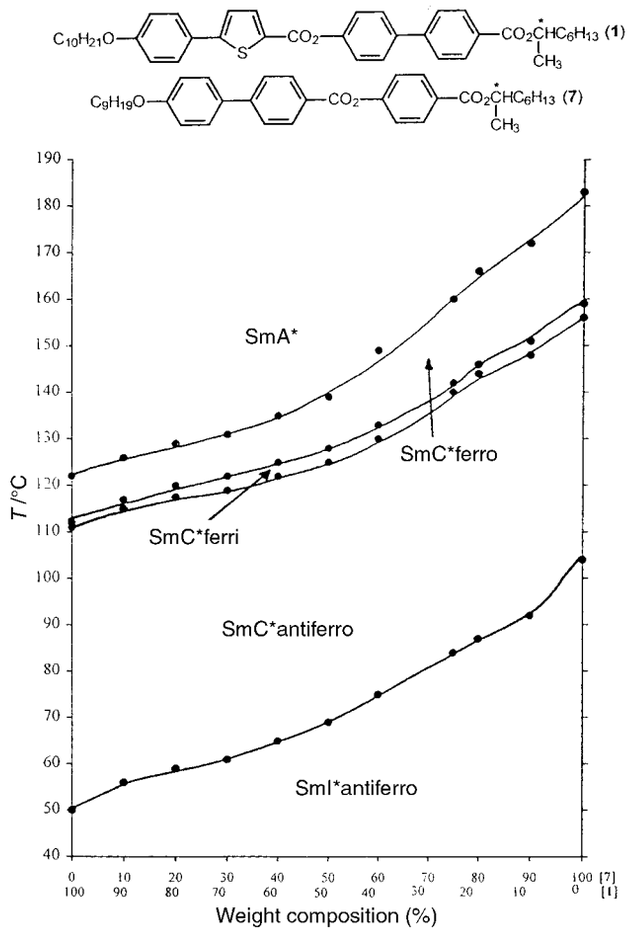

Fig. 7 Miscibility diagram for various compositions of (*S*)-4′-(1-methylheptyloxycarbonyloxy)biphenyl-4-yl 5-(4-*n*-decyloxyphenyl)-thiophene-2-carboxylate (**1**) with the standard (*S*)-1-methylheptyl 4-(4′-nonyloxybiphenyl-4-ylcarbonyloxy)benzoate (**7**).

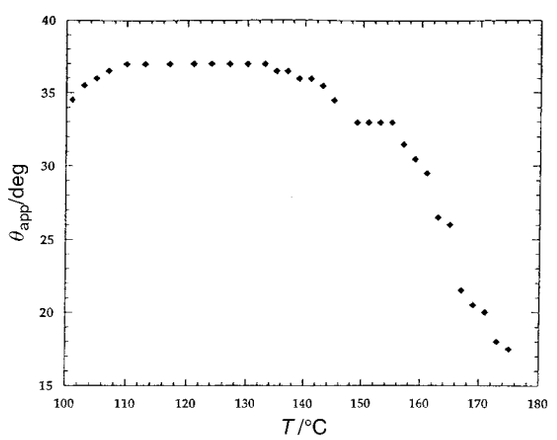

Fig. 8 Temperature dependence of the apparent tilt angle, θ_{app}, at an applied electric field of $E = 15$ V μm^{-1}.

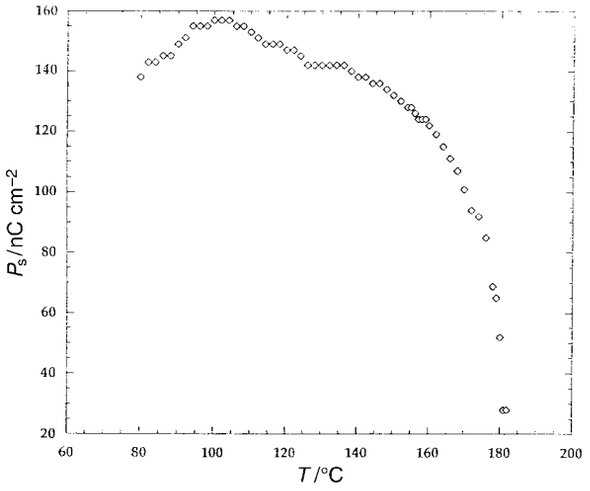

Fig. 9 Temperature dependence of the spontaneous polarisation, P_S, for a 2 μm thick sample.

Although the magnitude of this ratio is not 1 : 3 as readily described in the literature, the threshold behaviour of P_S in the ferrielectric phase was further examined by investigation of current hysteresis loops at lower and higher voltages with respect to V_C (Fig. 11).

Unfortunately, the classical single loop with tri-step character at low voltages was not observed due to the limitations of the instrument. The measurements have been made at a frequency of 4 Hz, which is still deemed too high for the ferrielectric state to be detected as it attempts slowly to relax back from the field-induced ferroelectric state. If a sufficiently low operating frequency could have been generated, such as 0.1 Hz, then a classical loop with tri-step character would be observed. Increasing the frequency to 1 kHz merely caused broadening of the hysteresis loop with no change in the magnitude of the polarisation.

The corresponding DSC data for the ferrielectric phase was re-examined to check for the possibility of subphases. Unfortunately, this was inconclusive because of the narrow temperature interval of the ferrielectric phase (1.3 °C) coupled with the weak second-order nature of the transition. The trace in this region is very diffuse, probably due to co-existence of phases, and in some parts indistinguishable from the background. However, possible occurrence of ferrielectric–ferrielectric transitions should not be discounted and a conoscopic or similar electric field study[13,14] on free-standing films may reveal further information.

Fig. 12–14 depict the current and optic response behaviour with respect to triangular-wave applied voltage. Classical

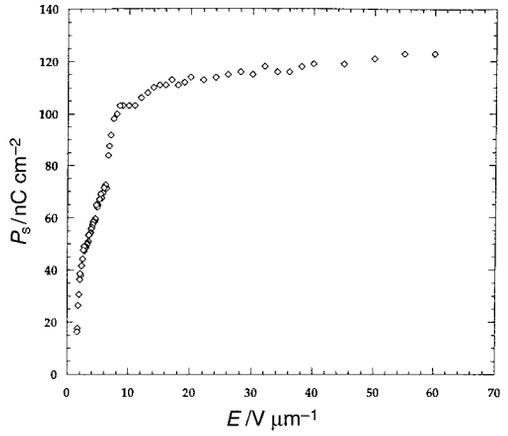

Fig. 10 Voltage dependence of P_S in the ferrielectric phase at 158.5 °C for a 2 μm thick sample.

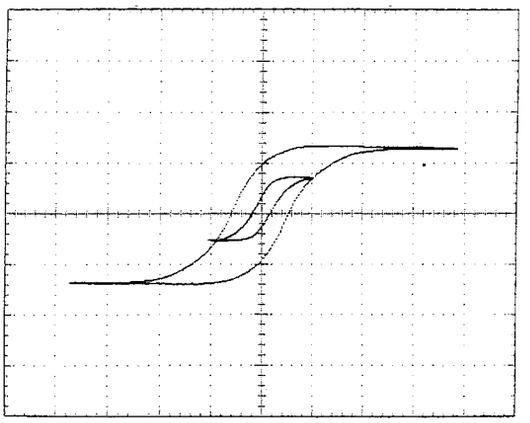

Fig. 11 Current hysteresis loops for the ferrielectric phase at $E=4$ V μm^{-1} (small loop) and $E=15$ V μm^{-1} (large loop) for a 2 μm thick sample.

results are not obtained, for example, the current peaks are asymmetric (Fig. 13) and the transmittance between the two peaks either side of the antiferroelectric state is non-identical. At present we cannot fully explain these unusual results, however, they may be due to the influence of strong liquid crystal–glass substrate boundary forces. Such interactions are well known to destroy ferri- and antiferro-electric ordering and promote ferroelectric ordering leading to unusual results. Also, there may be asymmetry in the surface treatment of both substrate surfaces, *i.e.*, the cell itself. Non-identical transmittance may be due to the fact that this material possesses an unusually high molecular tilt angle in the region of 33–38° in the ferri- and especially in the anti-ferroelectric state, *i.e.*, much larger than 22.5°.

Fig. 12 reveals the characteristics of the ferrielectric phase. The current response matches changes in optical response. However, notably, the current response does not fall to zero immediately (two very close peaks) which clearly discriminates from being either the ferro- or antiferro-electric phase. Thereafter, as the temperature is cooled and the antiferroelectric phase is established, two well separated peaks are observed for the current response which correspond to the antiferroelectric phase, *i.e.*, tristate switching (Fig. 13).

The SmI*antiferroelectric phase is characterised by the development of more current peaks, in our case there are three, each of them gives a corresponding optical response (Fig. 14). This behaviour may be attributed to a complex switching pattern of the antiferroelectric SmI*antiferroelectric phase. Goodby *et al.*[15] have reported similar complex switching behaviour for the SmI phase.

Surprisingly, as shown in Fig. 15, a linear electro-optic

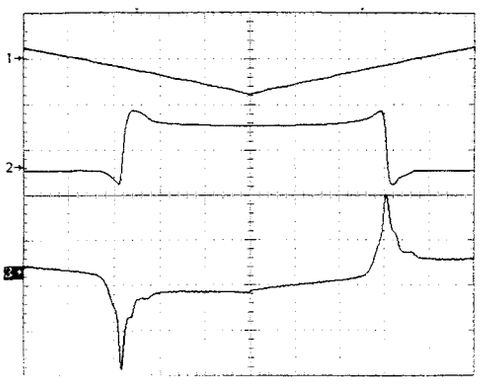

Fig. 12 Electro-optical and current response for a 2 μm thick sample in the ferrielectric phase when a voltage of $U_{PP}=40$ V and $f=0.1$ Hz is applied to the cell. The traces 1, 2 and 3 are the applied voltage, optic and current response, respectively.

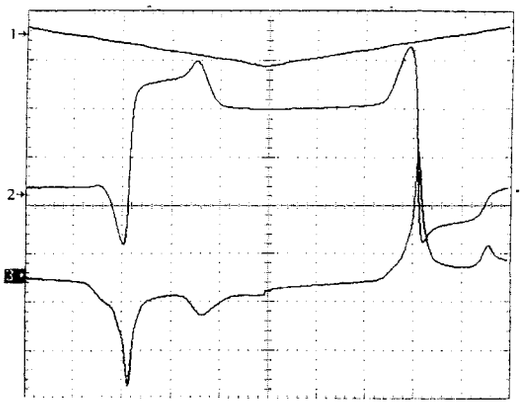

Fig. 13 Electro-optical and current response for a 2 μm thick sample in the antiferroelectric phase at 125 °C when a voltage of $U_{PP}=40$ V and $f=0.1$ Hz is applied to the cell.

response with a response time of approximately 200 μs (frequency, 100 Hz) was detected deep in to the so called *crystal phase* or high order smectic crystal phase, SmX. Since switching is detected it most likely corresponds to a high order smectic crystal phase and at present we cannot explain fully its origin and it is subject to extensive further investigation.

Experimental

Structural confirmation of the structures of the intermediates and products was obtained by ^{1}H NMR spectroscopy (JEOL FX60Q 270 MHz spectrometer) with tetramethylsilane as the internal standard and infrared spectroscopy (Perkin-Elmer FT 1605 spectrophotometer). Mass spectra were determined with a VG 7070E mass spectrometer. The specific optical rotation of compound **1**, dissolved in analytical grade $CHCl_3$, was determined at room temperature using a Perkin-Elmer 241 polarimeter and is given in 10^{-1} deg cm^2 g^{-1}. (*R*)-Octan-2-ol (ChiraSelect, ⩾99%) was purchased from the Aldrich Chemical Company and chiral phenol, **6**, was prepared according to the method reported by Booth *et al.*[6]

4-*n*-Decyloxyphenylboronic acid 3

In an inert atmosphere of nitrogen, commercial 1.6 M *n*-butyllithium (32 ml, 0.052 mol) was injected, dropwise, to a cooled (−78 °C), stirred, solution of 4-*n*-decyloxy-1-bromobenzene, **2**, (16 g, 0.051 mol) in dry tetrahydrofuran (100 ml) at such a rate that the temperature did not exceed −65 °C. After stirring for a further 2 h, trimethyl borate (22 ml, 0.194 mol) was injected and the solution was allowed to stir to room temperature overnight. The reaction mixture was then hydrolysed (4 M HCl) over a 1 h period. Subsequently, the crude product was extracted with diethyl ether, dried ($MgSO_4$) and the solvent removed *in vacuo* to yield the crude 4-*n*-decyloxyphenylboronic acid, **3**, (91%) as an off-white solid. A small amount of the boronic acid was purified by washing with hot petroleum ether (bp 60–80 °C) followed by recrystallisation from water to furnish the pure 4-*n*-decyloxyphenylboronic acid, **3**, as a white solid. However, the remainder was used as crude in the next step of the reaction scheme. $\delta_H(CDCl_3)$: 0.9 (3 H, t, CH_3), 1.2–1.5 (14 H, m, $(CH_2)_7$), 1.8 (2 H, quintet, $ArOCH_2CH_2$), 4.0 (2 H, t, $ArOCH_2$), 6.8 (2 H, d, ArH, $J=8$ Hz), 7.8 (2 H, d, ArH, $J=8$ Hz); IR ν_{max} (KBr) 3550–3200 (OH str.), 2920, 2850, 1605, 1465, 1411, 1351, 1251, 1171, 822 cm^{-1}; MS, *m*/*z*: 278 (M^+), 234 (10%), 94 (100%).

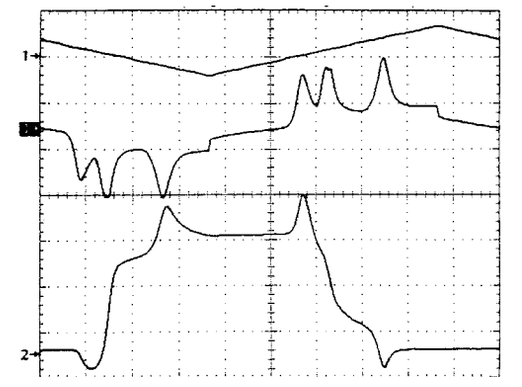

Fig. 14 Electro-optical and current response for a 2 μm thick sample in the SmI*antiferroelectric phase at 95 °C when a voltage of $U_{PP}=57$ V and $f=0.1$ Hz is applied to the cell.

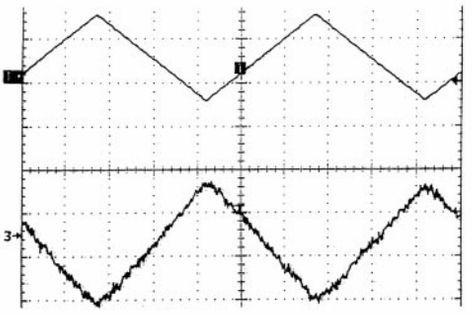

Fig. 15 Electro-optic response in the 'SmX' at 28 °C for a 2 μm thick sample when a voltage of $U_{PP}=200$ V and $f=106$ Hz is applied to the cell.

2-(4-*n*-Decyloxyphenyl)thiophene 4

A solution of crude 4-*n*-decyloxyphenylboronic acid, **3**, (8.8 g, 0.032 mol) in ethanol (20 ml) was added to a rapidly stirred mixture of 2-bromothiophene (5.2 g, 0.032 mol), tetrakis(triphenylphosphine)palladium(0) (0.5 g, 0.0004 mol), aqueous sodium carbonate (2 M, 30 ml) and 1,2-dimethoxyethane (30 ml). The mixture was heated under reflux until all the 2-bromothiophene had been consumed (monitored by thin layer chromatography). The reaction mixture was then cooled, extracted with diethyl ether, dried ($MgSO_4$) and the solvent removed *in vacuo*. The resulting brown solid was purified by flash chromatography on silica gel, eluting with 9 : 1 petroleum ether (bp 40–60 °C)–dichloromethane to afford the desired 2-(4-*n*-decyloxyphenyl)thiophene, **4**, 6.6 g (65%) as a pale yellow solid, 74 –77 °C: $\delta_H(CDCl_3)$ 0.9 (3 H, t, CH_3), 1.2–1.45 (14 H, m, $(CH_2)_7$), 1.8 (2 H, quintet, $ArOCH_2CH_2$), 4.0 (2 H, t, $ArOCH_2$), 6.9 (2 H, d, ArH, $J=8$ Hz), 7.05 (1 H, d, ThH, $J=4$ Hz), 7.19 (1 H, d, ThH, $J=4$Hz), 7.50 (2 H, d, ArH, $J=8$ Hz); IR ν_{max} (KBr) 2954, 2918, 2848, 1606, 1533, 1501, 1473, 1288, 1180, 1036, 854, 700, 681 cm^{-1}; MS, *m*/*z*: 316 (M^+, 100%), 176 (20%).

5-(4-*n*-Decyloxyphenyl)thiophene-2-carboxylic acid 5

In an inert atmosphere of nitrogen, commercial 1.6 M *n*-butyllithium (12 ml, 0.019 mol) was added dropwise to a stirred, cooled (−78 °C) solution of 2-(4-*n*-decyloxyphenyl)thiophene, **4**, (5.4 g, 0.017 mol) in dry tetrahydrofuran (50 ml) at such a rate that the temperature did not exceed −65 °C. The resulting mixture was stirred for a further 2 h, poured on to a large excess of solid carbon dioxide and allowed to stand overnight. The solution was acidified (4 M HCl), extracted with diethyl ether, dried ($MgSO_4$) and the solvent removed *in vacuo* to yield a green solid. The carboxylic acid was used in the next step without further purification. $\delta_H(CDCl_3)$ 0.9 (3 H, t, CH_3), 1.2–1.45 (14 H, m, $(CH_2)_7$), 1.8 (2 H, quintet, $ArOCH_2CH_2$), 4.0 (2 H, t, $ArOCH_2$), 4.5 (1 H, s, OH, disappears on D_2O shake), 6.9 (2 H, d, ArH, $J=8$ Hz), 7.2 (1

H, d, ThH, $J=4$ Hz), 7.60 (2 H, d, ArH, $J=8$ Hz), 7.82 (1 H, d, ThH, $J=4$Hz); IR ν_{max} (KBr) 3500–2950 (OH str.), 1702 (C=O str.), 1253, 1180, 814 cm^{-1}; MS, *m/z*: 360 (M^+, 2%), 176 (100%).

(*S*)-4′-(1-Methylheptyloxycarbonyl)biphenyl-4-yl 5-(4-*n*-decyloxyphenyl)thiophene-2-carboxylate 1

1,3-Dicyclohexylcarbodiimide (0.50 g, 0.0024 mol) and (*S*)-1-methylheptyl 4′-hydroxybiphenyl-4-carboxylate, **6**, (0.36 g, 0.0014 mol) were added to 5-(4-*n*-decyloxyphenyl)thiophene-2-carboxylic acid, **5**, (0.0014 mol) in dry dichloromethane (25 ml). 4-Dimethylaminopyridine (1–2 crystals) was added as catalyst and the reaction mixture was left to stir for 2 h at room temperature. The resultant white precipitate was removed by filtration and the filtrate was evaporated to dryness under reduced pressure. The crude residue was purified by flash chromatography on silica gel eluting with 1 : 1 petroleum ether (bp 60–80 °C)–dichloromethane followed by repeated crystallisation from ethanol to yield the desired (*S*)-4′-(1-methylheptyloxycarbonyl)biphenyl-4-yl 5-(4-*n*-decyloxyphenyl)thiophene-2-carboxylate, **1**, 0.9 g (64%), as an off-white solid. The liquid crystalline transition temperatures are listed in Table 1. Found: C, 75.41, H, 7.82%. $C_{42}H_{52}O_5S$ requires C, 75.45, H, 7.78%; δ_H ($CDCl_3$) 0.9 (6 H, t, $2\times CH_3$), 1.28–1.36 (12 H, m, alkyl), 4.0 (2 H, t, $ArOCH_2$), 5.1 (1 H, sextet, $C^*(H)CH_3$), 6.93 (2 H, d, ArH, $J=8$ Hz), 7.26 (1 H, d, ThH, $J=4$ Hz), 7.29 (2 H, d, ArH, $J=8$Hz), 7.59 (2 H, d, ArH. $J=8$Hz), 7.92 (1 H, d, ThH, $J=4$ Hz), 8.13 (2 H, d, ArH, $J=8$ Hz); IR ν_{max} (KBr) 2924, 2854, 1722(C=O), 1709(C=O), 1605, 1449, 1271, 1205, 1165, 1112, 1081, 1019, 831, 807, 761 cm^{-1}. MS, *m/z*: 668 (M^+, 15%), 539 (15%), 343 (100%), 203 (96%). $[\alpha]_D=11.9$ (*c*, 0.0016 g ml^{-1} in $CHCl_3$).

Conclusion

Complementary optical microscopy, differential scanning calorimetry, miscibility, and electro-optical and current response studies show clear evidence for the existence of the SmA*, SmC*ferroelectric, SmC*ferrielectric, SmC*antiferroelectric and SmI*antiferroelectric phase types in a novel bent-shaped chiral compound, namely: (*S*)-4′-(1-methylheptyloxycarbonyl)biphenyl-4-yl 5-(4-*n*-decyloxyphenyl)thiophene-2-carboxylate (**1**). Electro-optical switching is also observed in a so-called crystal phase which appears below the SmI*antiferroelectric phase. This is currently under further investigation together with elaborate pitch studies on the fingerprint texture of the SmC*antiferroelectric phase. The results of these studies will be published in a later communication.

Acknowledgements

ASM would like to thank the Royal Society of Chemistry for the award of a 'JWT Jones Travelling Fellowship' in order to participate in electro-optical characterisation at Chalmers University of Technology, Sweden, and the Engineering and Physical Sciences Research Council (research studentship for C.G.).

References

1 *17th International Liquid Crystal Conference, Program and Abstracts Book*, July 19–24, 1998, Centre National de la Recherche Scientifique, Université Louis-Pasteur de Strasbourg, Strasbourg, France.
2 A. D. L. Chandani, Y. Ouchi, H. Takezoe, A. Fukuda, K. Terashima, K. Furukawa and A. Kishi, *Jpn. J. Appl. Phys. Part 2*, 1989, **28**, 1261.
3 A. Fukuda, Y. Takanishi, T. Isokaki, K. Ishikawa and H. Takezoe, *J. Mater. Chem.*, 1994, **4**, 997.
4 W. K. Robinson, H. Gleeson, M. Hird, A. J. Seed and P. Styring, *Mol. Cryst. Liq. Cryst.*, 1997, **299**, 19.
5 D. J. Byron, L. Komitov, A. S. Matharu, I. McSherry and R. C. Wilson, *J. Mater. Chem.*, 1996, **6**(12), 1871.
6 C. J. Booth, D. A. Dunmur, J. W. Goodby, K. S. Jaskaran and K. J. Toyne, *J. Mater. Chem.*, 1994, **4**(5), 747.
7 N. Miyaura, T. Yanagi and A. Suzuki, *Synth. Commun.*, 1981, **11**, 513.
8 A. Hassner and V. Alexanian, *Tetrahedron Lett.*, 1978, 4475.
9 C. Loubser, P. L. Wessels, P. Styring and J. W. Goodby, *J. Mater. Chem.*, 1994, **4**(1), 71.
10 E. Gorecka, M. Glogarova, H. Sverenyak and L. Lejcek, *Ferroelectrics*, 1996, **178**, 101.
11 A. J. Seed, M. Hird, P. Styring, H. Gleeson and J. T. Mills, *Mol. Cryst. Liq. Cryst.*, 1997, **299**, 19.
12 G. Andersson, PhD Thesis, 1992, Chalmers University, Göteborg, Sweden.
13 E. Gorecka, A. D. L. Chandani, Y. Ouchi, H. Takezoe and A. Fukuda, *Jpn. J. Appl. Phys. Part 1*, 1990, **29**(1), 131.
14 K. Itoh, M. Kabe, K. Miyachi, Y. Takanishi, H. Takezoe and A. Fukuda, *J. Mater. Chem.*, 1997, **7**(3), 407.
15 J. W. Goodby, J. S. Patel and F. M. Leslie, *Ferroelectrics*, 1984, **59**, 137.